A Sealability Study on Bismuth-Tin Alloys for Plugging and Abandonment of Wells

Lewaa Hmadeh[1]*, Andriani Manataki[1], Marcelo Anunciação Jaculli[1], Behzad Elahifar[1], and Sigbjørn Sangesland[1]

[1]Department of Geoscience and Petroleum, Norwegian University of Science and Technology

Summary

The use of bismuth alloys as a barrier material for plugging and abandonment (P&A) has gained traction in the literature due to the large number of wells scheduled to be plugged and abandoned. In addition, many questions have been raised regarding the sealing efficiency of cement in the long run. Within this context, this work performs a thorough study of the sealability of plugs made with the eutectic bismuth-tin alloy. This effort is divided into three fronts: laboratory tests to verify the pressure resistance and leakage rate of these plugs, microscopy analyses to corroborate the tests' insights through observations of the alloy microstructure, and numerical simulations to capture and model the involved phenomena aiming to reproduce real well scenarios in the future. Results show that bismuth-tin plugs exhibit better pressure resistance and lesser leakage rates than cement plugs, which indicates that this material is a suitable candidate. Better sealing properties are achieved when the plugs are set under higher curing pressures than the atmospheric pressure, an observation that is confirmed when observing the microstructures formed. Finally, a suitable material model that captures the expansion upon solidification is proposed, and the effect of thermal expansion on the plug and pipe assembly is observed.

Introduction

P&A of wells has always been an expensive and time-consuming operation. Historically, P&A operations were usually less thought of during the early planning of drilling projects. Consequently, as soon as the economic life cycle of a well comes to an end, operators follow existing guidelines to plug the well while making sure to meet the regulatory requirements. Following such traditional approaches has led to integrity problems, potentially resulting in leakage from the abandoned well. The main component of abandonment practices is Portland cement, which is currently the most conventional and acceptable well-sealing material according to the *NORSOK D-010* (2021). Despite being regarded as a qualified sealing material by regulators, integrity problems have been noted considering the desired long-term abandonment perspective, thus questioning its sealing capability. The sealing integrity of a cement plug weakens due to various downhole temperature and pressure conditions, such as cracking and debonding from the casing in high-pressure and high-temperature environments or being vulnerable to corrosion in sour environments (Vrålstad et al. 2015, 2016). Such properties favor the creation of microannuli, which become migration paths for downhole fluids.

Many abandoned wells are currently leaking mainly because of poor cementing jobs (Dusseault et al. 2000; Roijmans et al. 2023; Vrålstad et al. 2019). Thus, the focus on finding an alternative to cement has become more serious and more urgent than before. Every year, the Norwegian Oil and Gas Association (now Offshore Norge) sets a roadmap for new P&A technologies in which they highlight key actions needed to achieve safe, cost-effective, and environmentally friendly P&A operations. Ever since 2015, finding an alternative to cement has always been there **(Fig. 1),** meaning that an adequate alternative sealing material has not been found yet. The urge to find a new alternative is becoming more evident with the "Plug Wave" our world will soon be facing. FloPetrol Well Barrier AS reported more than 4,000,000 wells to be plugged in the near and long future, with more than 500,000 wells to be drilled within the next 3 to 5 years (Hetlevik 2022).

The alternative must not only cut P&A operational costs (including decreasing rig time) but also guarantee a long-lasting seal capable of isolating hydrocarbon-producing zones and/or aquifers. In this context, bismuth metal alloys appear as an alternative potential for fulfilling this purpose. Bismuth (Bi) is a metal with a melting point of 273°C and possesses many properties that render it an effective sealing material for permanent P&A operations. First, it is impermeable compared to cement, which reduces the risk of leakage through the plug. In its liquid (melted) state, bismuth has a high density that eases the displacement of well fluids. It can easily invade the smallest pores and notches with a viscosity equivalent to that of water, thus averting the need for surface pumping or pressure application. When melted, the bismuth takes the shape of the casing it is being set in, making it independent of the geometry and any existing deformations in the installation area. Upon solidification, bismuth undergoes a significant expansion; pure bismuth can expand by approximately 3% in volume (Carragher et al. 2019; Fulks and Carragher 2021; Mackenzie et al. 2022), similar to how water expands as it becomes ice. As solidification first takes place at the top and bottom of the plug, the bismuth is forced to expand radially. This expansion feature is the main sealing mechanism that holds the plug in place. Further, bismuth is corrosion-resistant to H_2S and CO_2, which is a valuable feature for P&A applications (Carragher and Fulks 2018; Fulks and Carragher 2021; Mackenzie et al. 2022; Thorstensen et al. 2022; Zhang et al. 2020, 2021a).

However, pure bismuth is not adequate to be a standalone sealing barrier due to its brittle nature and high melting point (273°C) in comparison to what can be managed safely downhole. In addition, its eutectic property leads to instant solidification as soon as the temperature drops below its melting point. Thus, there is a chance that the bismuth plug might not be positioned at the desired depth before it solidifies. Carragher and Fulks (2018) successfully developed bismuth alloys with melting temperatures ranging from 93 to 263°C, and they were able to show through extensive testing that the alloys exhibit similar properties to that of pure bismuth such as high density, low viscosity, expansion upon solidification, low toxicity, and corrosion resistance. Placement is performed using wireline and in combination with thermite technology to melt it. The most common type of alloy currently used in practice is the eutectic bismuth-tin alloy (BiSn),

*Corresponding author; email: lewaa.hmadeh@ntnu.no

Original SPE manuscript received for review 25 October 2023. Revised manuscript received for review 23 February 2024. Paper (SPE 219744) peer approved 18 March 2024.

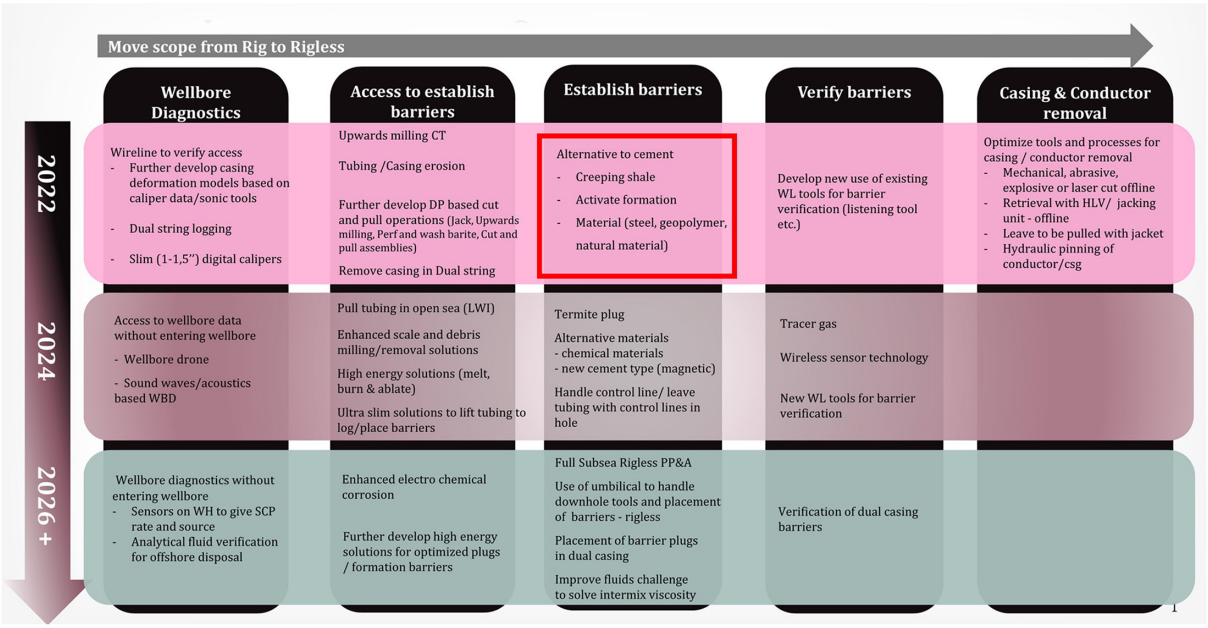

Fig. 1—Roadmap for new P&A Technologies (Offshore Norge 2021).

with a melting point of 138°C. Because the alloy contains 58% bismuth and 42% tin, it expands by approximately 0.77% upon solidification (Goodrich 1929).

The objective of this article is to delve into the mechanical properties and behavior of bismuth-tin alloy plugs. This is achieved through three fronts: laboratory tests to verify its sealability in terms of leakage rate and capability of withstanding pressure; microscopy analyses using a SEM (scanning electron microscope) to verify what happens with the microstructure of the alloy when solidified under different conditions; and numerical simulations to capture the expansion phenomenon and propose a suitable material model for further studies. Laboratory tests show that the bismuth plug performed better than cement in terms of leakage rate and pressure resistance, considering our small-scale laboratory setup, with these results being further supported by the SEM analysis and the simulations. We conclude that bismuth is a promising material that must be investigated further until its eventual acceptance as an alternative barrier material by the *NORSOK D-010* (2021) standard.

Methodology

Materials Used. The primary materials of relevance are bismuth-tin alloy blocks, Portland G cement, steel X-52 pipe, and casting sand. Detailed properties of the listed materials are presented below. The chosen low-melting-point alloy was "MCP 137" composed of ~58% bismuth and ~42% tin (5N Inc 2012), which corresponds to the eutectic point. The properties of the eutectic bismuth-tin alloy are presented in **Table 1.** Properties of bismuth-tin alloys are available in the literature in several works as previously collected by Hmadeh et al. (2024).

Property	Eutectic Bismuth-Tin Alloy (Bi58-Sn42)
Density	8.56 ~ 8.73 g/cm^3
Young's modulus	42.72 ~ 43 GPa
Poisson's ratio	0.3426
Yield strength	50 ~ 70 MPa
Ultimate strength	70 ~ 80 MPa
Melting point	135 ~ 139 °C
Coefficient of thermal expansion	15 ~ 17 μm/(m · °C) @ 20 ~ 90°C
Linear expansion after casting (observed at 20°C)	0.015% @ 1 hour 0.03% @ 3 hours 0.045% @ 8 hours 0.06% @ 1 day 0.07% @ 3 days 0.08% @ 10 days 0.09% @ 1 month 0.095% @ 3 months 0.1% @ 12 months

Table 1—Properties of the eutectic BiSn alloy.

The cement system chosen for this study was a mixture of Portland Cement Class-G (provided by NORCEM AS) and water without any additives. The steel X-52 pipe (Rolf Lycke AS 2012) was chosen as it had similar properties to that of casings and tubings used in oil and gas wells and was easily available, thus making it a suitable replacement for a small-scale test. The pipes were cut into 250-mm long sections with an inner diameter of 53.35 mm and an outer diameter of 60.80 mm. Its properties are provided in **Table 2.**

Property	Steel X-52
Density	7.84 g/cm^3
Young's modulus	212 GPa @ 20°C 207 GPa @ 100°C 200 GPa @ 200°C 193 GPa @ 300°C 185 GPa @ 400°C 176 GPa @ 500°C
Poisson's ratio	0.284 @ 20°C 0.287 @ 100°C 0.291 @ 200°C 0.295 @ 300°C 0.299 @ 400°C 0.303 @ 500°C
Yield strength	358 MPa
Ultimate strength	500 MPa
Coefficient of thermal expansion	12 μm/(m·°C) @ 20°C 12 μm/(m·°C) @ 100°C 13 μm/(m·°C) @ 200°C 13 μm/(m·°C) @ 300°C 14 μm/(m·°C) @ 400°C 14 μm/(m·°C) @ 500°C

Table 2—Properties of the steel X-52 (Rolf Lycke AS 2012).

Experimental Procedures. ***Cement Plug: Setting Process.*** The Portland G cement plug was mixed according to API Recommended Practice 10B-2 (*API RP 10B-2* 2013) and was prepared in collaboration with SINTEF, Drilling & Wells. The cement samples were set in an X-52 metal pipe and had a minimum of 5 days to cure, which has been decided according to an internal experience at SINTEF. The cement was not immersed in a water bath during curing. Each cement plug had a length of 185 mm. A gap of 65 mm from the top was left empty. It should be noted that the cement used in this study does not represent the actual cement being used in practice, as cement plug mixtures normally include expansion additives (e.g., magnesium oxide) or inert fillers (e.g., glass beads). Considering that the research focuses on the characteristics of an unmodified bismuth-tin eutectic alloy, the decision was made to use pure Portland G cement as the initial reference point for our experiments.

Bismuth Alloy Plug: Melting and Setting Process. The bismuth alloy (MCP-137) was first received from the manufacturer in the form of solid circular blocks, which were then melted in steel containers using an electric oven set at 200°C. After complete melting of the blocks was ensured, the molten bismuth was poured into dry pipe samples over a compacted sand foundation. The alloy plug samples used in our experimentation were filled with 95 mm of dry casting sand, above which molten bismuth alloy was poured and left to solidify at standard conditions. Such sand tends to stick together, avoiding seepage of the molten alloy into it. As the alloy used has a high density of 8.58 SG, it was essential to establish a foundation capable of supporting its liquid form; otherwise, the liquid alloy would naturally descend. In practice, a mechanical bridge plug would be needed for the proper placement of the alloy plug. The plug length is 121 mm, which is shorter than that of the cement plug prepared (185 mm). A gap of 34 mm from the top was left for experimental purposes. **Fig. 2** shows the plug-pipe setup for both the bismuth alloy and cement samples.

It is crucial to emphasize that using a wet pipe for such experiments was not practical due to safety concerns associated with an explosive reaction triggered by the rapid vaporization of water. Upon contact between the molten alloy and the water droplets on the inner surface of the pipe, a swift solidification of the alloy was witnessed accompanied by intense water vaporization. Consequently, an explosive incident occurred, causing the alloy to splatter beyond the confines of the pipe. Therefore, only dry pipes were used during the casting process.

In this work, we conduct tests on two bismuth alloy samples. Sample 1 is the one left to solidify and cure for 48 hours at standard conditions, whereas Sample 2 is left to solidify and cure for 48 hours under 40 bar of pressure at room temperature. Sample 2 is prepared following the methodology described by Hmadeh et al. (2023a). We reinforce that the plug strength increases over time as it keeps expanding until reaching a maximum value for very long times. 48 hours was selected during our initial tests as a reasonable compromise between attaining good resistance vs. keeping the testing time frame reasonable.

Hydraulic Push-Out Test. The primary aim behind conducting a hydraulic push-out test was to test the hydraulic shear bond strength of the plug samples prepared. The hydraulic bond strength is the minimum pressure required by an injection fluid to cause the plug-casing/formation interface to leak or detach. In our study, the injection fluid chosen was water. **Fig. 3** displays the test setup used, which in turn consists of the following:

1. A beaker filled with water.
2. "Test cell": a collective term for the pipe with the plug set inside, a steel cap on each end of the pipe, and four bolts. The bolts run along the sides of the pipe, penetrate the edges of both caps, and are tightened with eight steel nuts from both ends to ensure that the cell remains securely sealed after being subjected to high pressures. The test cell has a bottom outlet, which we keep open during the testing phase to create differential pressure between the top and the bottom of the plug.

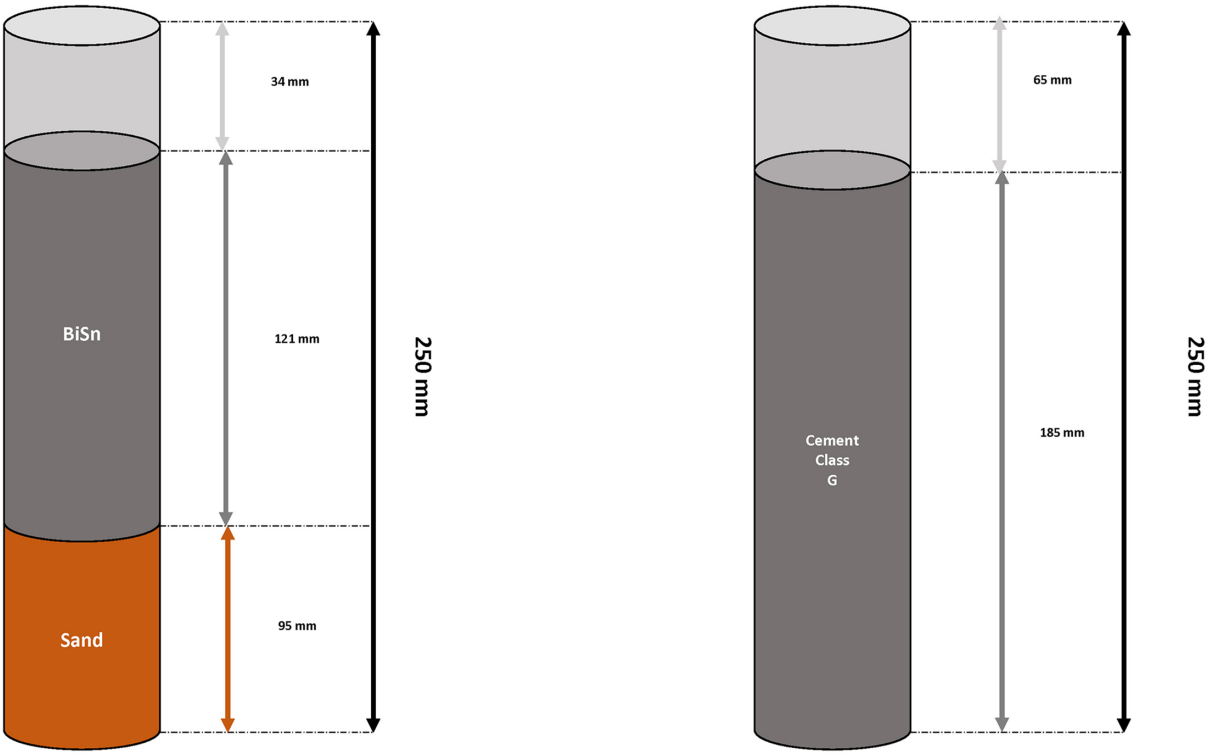

Fig. 2—Plug-pipe setup: bismuth alloy (left) and cement (right).

3. A dual cylinder hydraulic pump (VP-12K): the pump has various pumping modes depending on the operation the user defines. The steel rod connected to the top of the test cell is the water outlet of the pump, and the black wire immersed in the water beaker is the water inlet.

The pressure above the plug will be raised by the pump as it continuously pumps water at a predetermined rate. Eventually, the plug will fail after its sealing threshold has been reached, and it will displace downward. At the same time, a pressure drop will be witnessed as the hydraulic bond fails, where small gaps called microannuli will be opened through which water will make its way to the bottom outlet of the test cell. The test is halted once water starts to break through the bottom outlet.

Leakage Test Using Nitrogen Gas. Similarly, the leakage test aims to test the hydraulic bond strength, but the only difference here was the injection fluid used, which was nitrogen gas. With the test setup used, it was possible to quantify the leakage rates with the flow meters mounted on the setup. The small-scale laboratory setup used is shown in **Fig. 4.**

Setup Description. The current study used a compact laboratory setup, as depicted in **Fig. 4**. It mainly consists of a test cell housing a plug (either bismuth or cement) with both ends enclosed by steel caps connected to gas inlets. The setup was interconnected with a pressurizing system, flowmeters, and an automated data acquisition system that reads and records measurements every 10 seconds. The red dashed lines are electronic cables transferring data from sensors to the logging system. The pressure system was equipped with a nitrogen supply and pressure regulators to ensure control.

Before starting the test, Valve 1 was closed to establish a bypass line for gas to pass through the test cell. The top and bottom pressure lines connected to the test cell were regulated independently. The pressure on both ends of the plug was set to 20 bar, which is the maximum pressure the setup can withstand. The entire setup was tested for any leakage before the start of the experiment. Afterward, the pressure on the top side of the test cell was gradually decreased (according to an internal procedure by SINTEF), whereas the pressure at the bottom side was kept constant (20 bar). As a result, a differential pressure was created across the plug. The first indication of a gas leak was observed in the flowmeter reading, indicating the failure of the plug. The test was continued until a differential pressure of 20 bar was reached. The data of interest from this experiment is the breakthrough pressure and the leakage flow rate of the plug samples tested.

Microstructure Characterization. For microstructure characterization, two new bismuth plug samples were prepared according to the aforementioned setting methodology. Again, Sample 1 was left to cure under atmospheric pressure for 48 hours and Sample 2 was left to cure under 40 bar of pressure for 48 hours. A 3-mm disk was then cut from the middle section of each sample, as shown in **Fig. 5.** The disk was then divided into four quarters from which the ¼ was taken for preparation for microstructural characterization. Both samples were mechanically ground with abrasive media to a 0.04-μm colloidal silica surface finish. Silicon carbide particles have the tendency to be removed from the paper and embedded in the soft surfaces of both phases of the BiSn eutectic alloy. For this reason, the samples were ultrasonically cleaned in alcohol after each grinding step. After grinding, two steps of polishing were followed, using 3 μm and then 1 μm diamond particles. Specimens were then analyzed by scanning electron microscopy. A SEM-Hitatchi SU-6600 was used and operated at 25 kV, and electron micrographs were collected in the backscattered electron mode.

Numerical Simulations. Numerical simulations are conducted using the Ansys software package, which allows a wide variety of simulations, including structural and thermal analyses. The goal is to investigate different scenarios by varying properties, configurations, boundary conditions, etc. Simulations can be carried out for the two main scenarios: reproduction of laboratory tests and simulation using

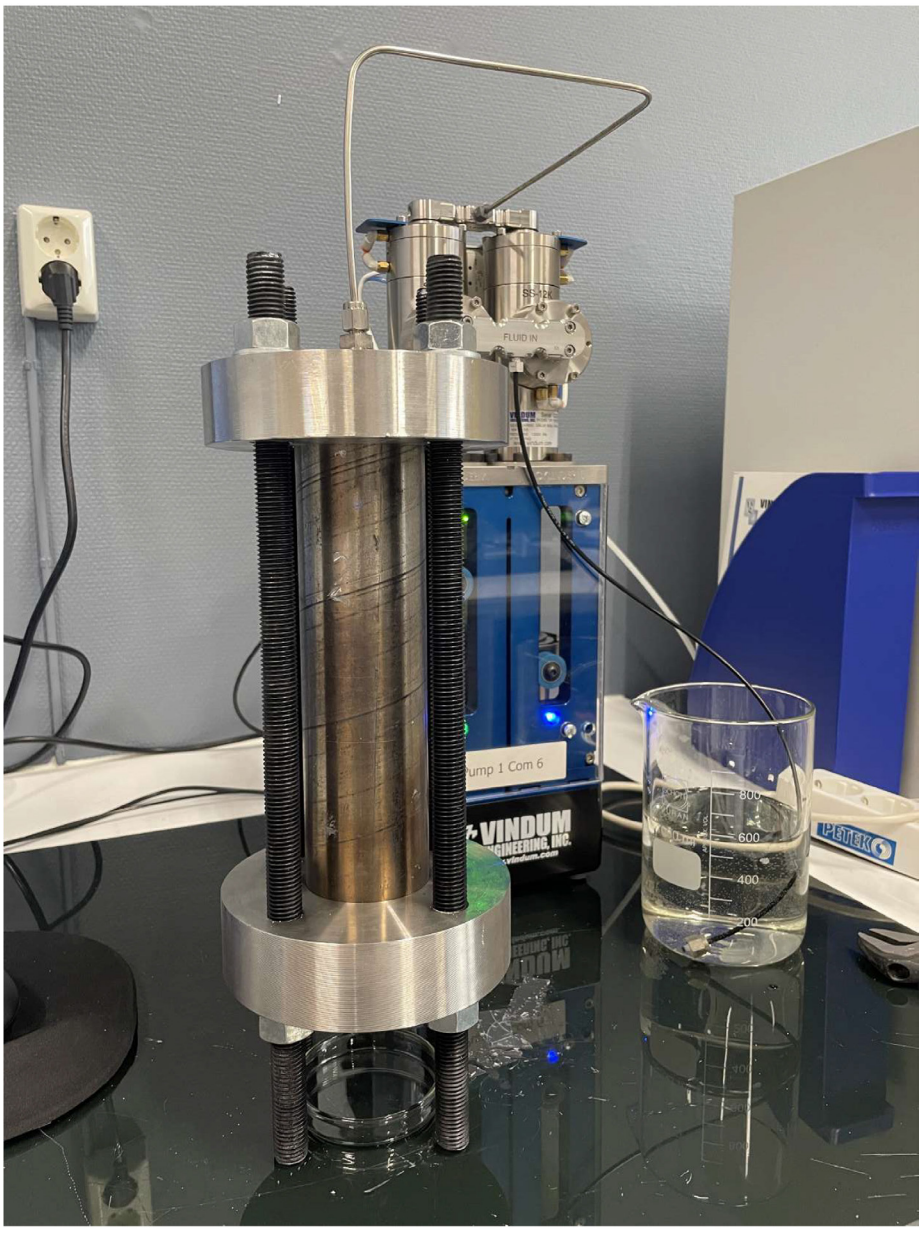

Fig. 3—Hydraulic push-out test setup.

field conditions. If a material model that follows the behavior observed in the laboratory is proposed, then real well scenarios may be simulated later with more confidence. Thus, the focus of this work is to start building this model and reproduce some of the laboratory results.

Based on experimental and numerical observations, the behavior under loads of the eutectic bismuth-tin alloy can be characterized by mainly three combined phenomena:

- The alloy expands during its solidification, which is unique to few metals in the periodic table. However, this expansion does not happen instantaneously when the material crosses the melting point, as some residual expansion may happen over time according to manufacturers' spreadsheets (5N Inc 2012).
- Creep effects, which are more relevant at higher temperatures closer to the melting point. The creep of the plug's alloy indicates that curing it under pressure and for longer times is important to guarantee adherence to the pipe's inner wall, which results in higher adhesion. This is an important consideration as the bismuth-tin alloy has a higher coefficient of thermal expansion than steel, and thus the plug would simply detach from the pipe if this assembly were to be cooled together.
- Aging effects, which lead to a weakening of the material properties due to high load at high temperatures and extended periods of time. This is a known effect for other metal alloys, such as aluminum (Kilic et al. 2019) and steel (Zhang et al. 2021b), and thus it is expected that this would also affect bismuth-tin alloys. This effect contraposes the creep effect as it is triggered by the same conditions (load, temperature, and time) but is detrimental to the material.

The uniqueness of this problem comes from the fact that the bismuth alloy is melted downhole, and then it expands when solidified. This phenomenon must be captured into the material model that is inserted into Ansys. Based on Khairulin et al. (2010), we know that the density changes from $\rho_i = 8.64$ g/cm^3 to $\rho_f = 8.57$ g/cm^{3}due to the solidification at the melting point (138°C). Thus, the resulting volumetric strain is:

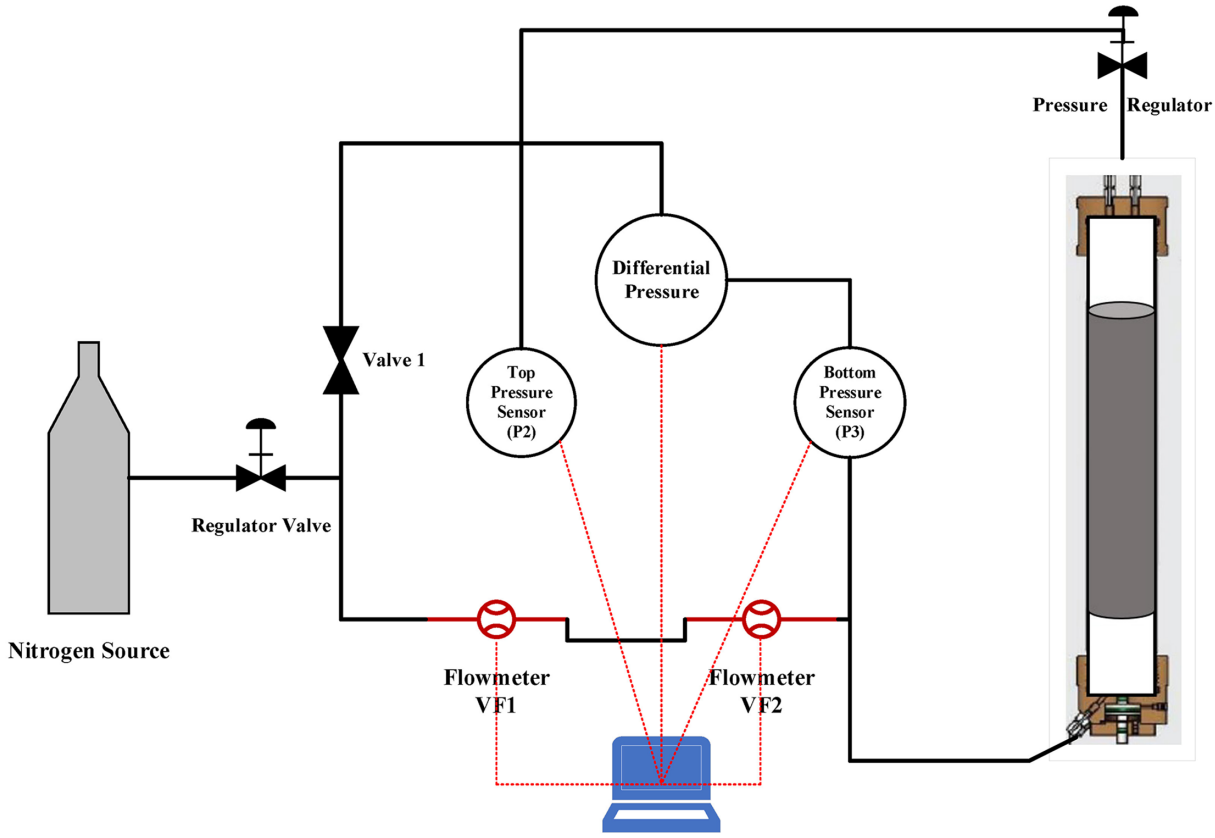

Fig. 4—Leakage test setup.

$$\varepsilon_{V,sol} = \frac{1/\rho_f - 1/\rho_i}{1/\rho_i} = \frac{1/8.57 - 1/8.64}{1/8.64} = 0.008168. \quad (1)$$

We propose that the alloy is allowed to expand when crossing the melting point, experiencing the aforementioned volumetric strain. This approach is valid because the thermal strain is independent of the temperature path, but it is dependent only on the current body temperature. It is important to note that the bismuth alloy keeps expanding over time, even days after solidifying; however, we simplify this to consider that the expansion happens instantaneously. Converting the volumetric strain to linear strain:

$$\varepsilon_{L,sol} = \frac{\varepsilon_{V,sol}}{3} = \frac{0.008168}{3} = 0.002723. \quad (2)$$

Once solid, the alloy behaves like any other metal alloy: it expands when heated and contracts when cooled down. A value of $\alpha_L = 0.000016\ °C^{-1}$ @ 20 °C has been provided for the solid phase as the coefficient of thermal expansion. The suggestion here is to add the linear strain to the thermal strain that the alloy experiences when heating from the reference temperature up to the melting point. If the solid alloy was to be heated from the zero-thermal-strain reference temperature T_{ref} (20°C) up to the melting point T_{mp} (138°C), the thermal strain $\varepsilon_{TH,mp}$ would be

$$\varepsilon_{TH,mp} = \alpha_L \left(T_{mp} - T_{ref}\right) = 0.000016 \cdot (138 - 20) = 0.001888. \quad (3)$$

Thus, we can find a new zero-thermal-strain reference temperature $T_{ref,new}$ as being

$$T_{ref,new} = T_{mp} - \frac{\varepsilon_{L,sol} + \varepsilon_{TH,mp}}{\alpha_L} = 138 - \frac{0.002723 + 0.001888}{0.000016} = -150.2\ °C. \quad (4)$$

Therefore, the only modification to the material model is changing the zero-thermal-strain reference temperature to this new value, guaranteeing that there will be a residual strain even if the plug is brought toward the former reference temperature. With this material model, we can successfully capture the alloy expansion and then see a contraction of the alloy as it cools down toward an equilibrium with the well temperature.

Results and Discussion

In this section, results are presented for the laboratory tests, SEM analysis, and numerical simulations.

Hydraulic Push-Out Tests. The objective of this section is to compare the pressure resistance of cement and bismuth plugs, and thus both plugs are tested under increasing hydraulic pressure. First, a 185-mm long cement plug was tested at standard conditions after being

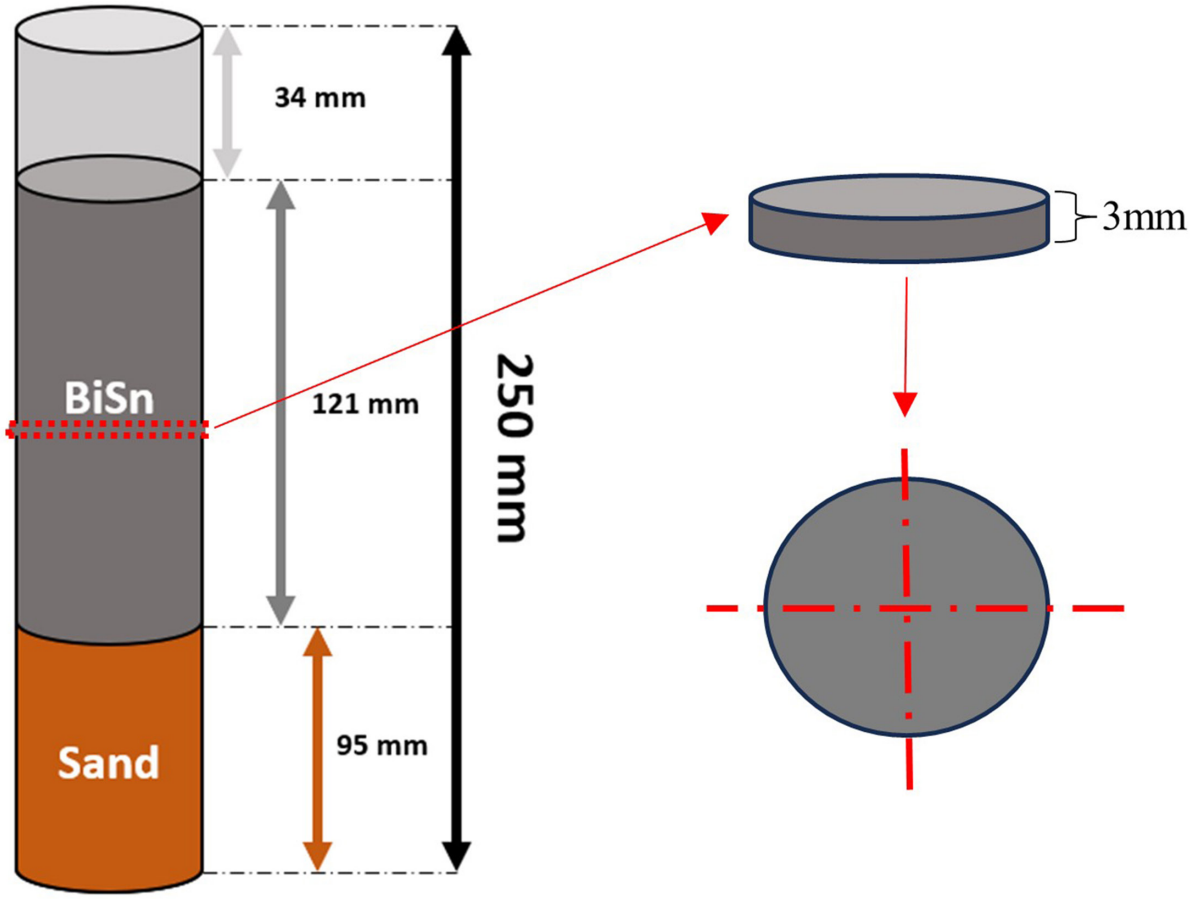

Fig. 5—Sample extraction procedure.

left to cure for 5 days. The hydraulic pump was set on paired rate delivery mode for continuous pumping of water at a predefined rate. In this case, the chosen pumping rate was 0.2 mL/min. The test results are presented in **Fig. 6.** At 6.32 bar, the cement plug was deemed to have failed hydraulically, with the sudden pressure drop indicating the creation of microannuli allowing water to flow through the plug-pipe interface. Then, the graph flattens out, indicating a constant flow of water through the created microannuli. A slight pressure drop was witnessed at 3.5 bar, which could be the result of water starting to create/open the microannuli at the top of the plug. In addition, to corroborate this result, another cement plug sample was subjected instead to a mechanical push-out test, which failed similarly at 5.73 bar.

Subsequently, the same push-out test was carried out on two 121-mm bismuth alloy samples. The only difference between these two samples was the setting pressure under which the plug solidified: Sample 1 at 1 bar (atmospheric pressure) and Sample 2 at 40 bar. The two tests were then repeated to confirm the observations, showing similar results. The results of these two samples are conveyed in **Fig. 7.**

The results presented in **Fig. 7** convey two different peaks at which the alloy plugs hydraulically failed. Sample 1, solidified and cured at standard conditions, failed at 67 bar, whereas Sample 2, solidified and cured under 40 bar of pressure and at room temperature, failed at 106 bar. This difference in results is attributed to the methodology of curing and solidifying the plug. Previous research (Hmadeh et al. 2023a, 2023b) indicated that setting the plug under pressure will enhance the radial expansion against the walls of the tubing, thus providing better bond strength. Meanwhile, setting a plug under atmospheric pressure favors the axial expansion of the plug as the alloy will naturally expand in the direction with the least resistance, which in this case will be upward in the axial direction. Therefore, the bond strength achieved under atmospheric pressure is weaker than that obtained under 40 bar of pressure (a difference of roughly 39 bar). This theory was also highlighted by Eden (2005), where the author claims that "if the material is allowed to cool in a manner in which it is not constrained, much of the expansion which occurs on cooling results in axial displacement of the remaining molten material rather than expansion in the radial direction to press against the well wall." Comparing the results shown in **Fig. 8** to the hydraulic bond strength of a neat Portland G cement depicted in **Fig. 6** and taking the worst-case scenario with a plug axially expanding (Sample 1: 67 bar), it is observed that the bismuth alloy sample was around 10 times more robust than the cement sample under the aforementioned testing conditions. This outcome is applicable solely within the context of the selected plug-length scale. To accurately extend laboratory findings to actual wellbores, a thorough scalability analysis is required.

Leakage Tests Using Nitrogen Gas. The leakage test was conducted on a 185-mm cement sample at atmospheric conditions. The results are presented in **Fig. 8**. As the differential pressure was changed manually using a manual regulator valve, sudden spikes in the volume flow rate were recorded. Thus, it was decided to report the moving average of the results to smooth these fluctuations in the recorded flow data.

The hydraulic shear bond failure was recorded at a differential pressure of 0.83 bar, as this was the pressure at which the flowmeters started to detect a flow of nitrogen gas. This early failure of the plug was expected since Opedal et al. (2018) conducted a similar experiment using the very same setup described. The cement system described by Opedal et al. (2018) detected flow at a differential pressure of 0.04 bar. Our experimentation yielded outcomes that displayed a nonlinear trend between the applied differential pressure and the

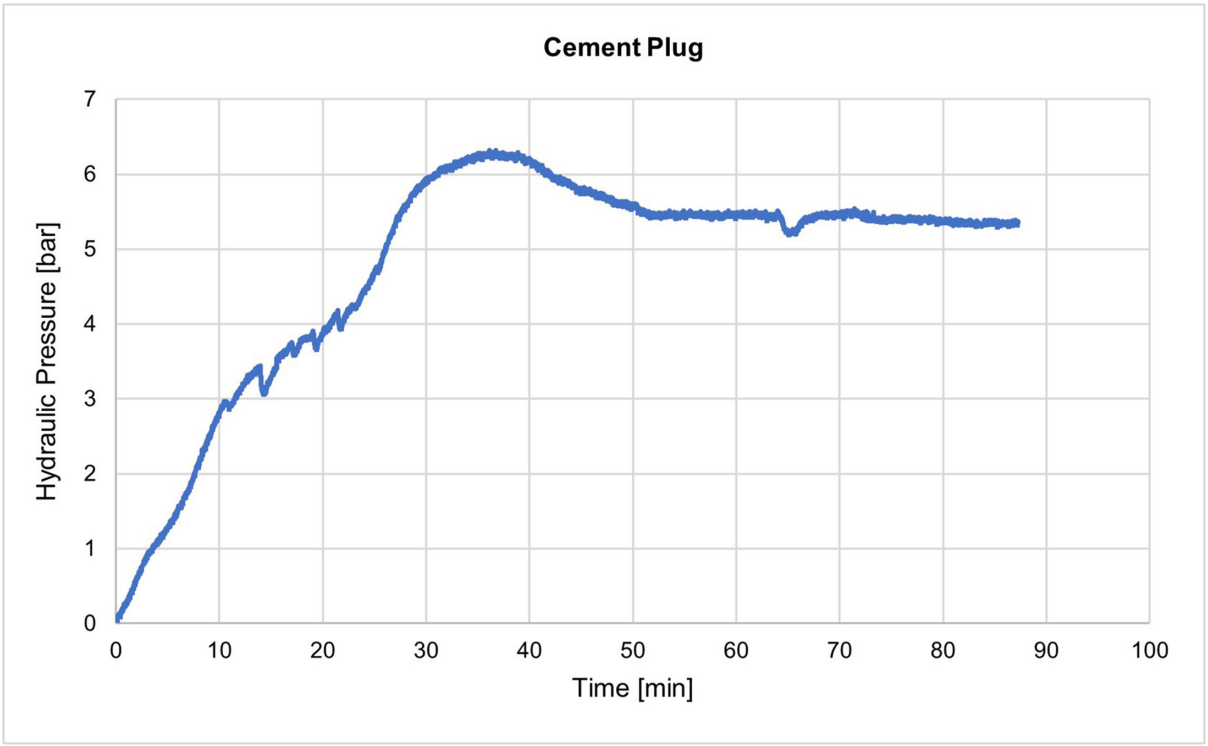

Fig. 6—Hydraulic push-out test results for a cement plug (Hmadeh et al. 2023b).

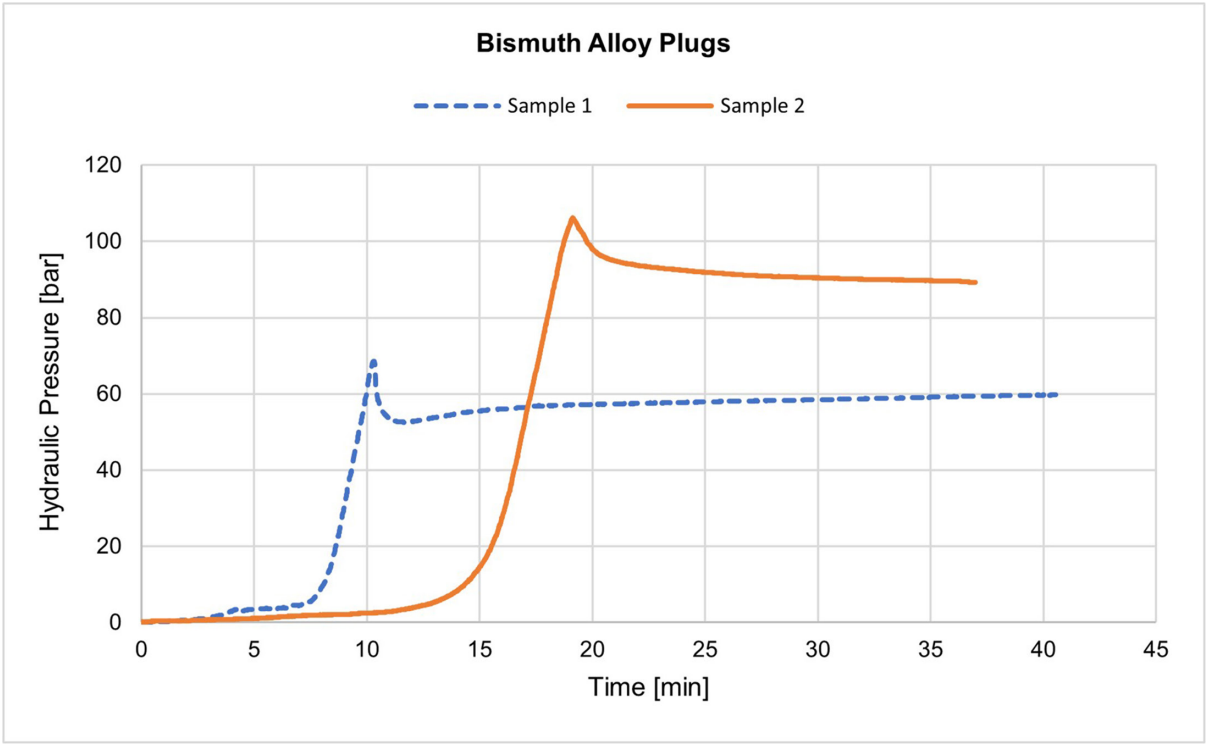

Fig. 7—Hydraulic push-out test results for bismuth alloy plugs (curing pressures: Sample 1 at 1 bar and Sample 2 at 40 bar).

measured flow, where it seems that the gap size between the cement plug and the pipe is increasing with increasing pressure, resulting in a higher flow rate as depicted in **Fig. 8**. Our test results align to a certain extent with the trend shown by Opedal et al. (2018), especially from the start of the experiment until 1.5 bar of differential pressure. However, it is also important to highlight that these two tests cannot be compared as Opedal et al. (2018) used a longer cement plug (400 mm) which was cured at 20 bar and 66°C for 5 days and set in a thicker pipe with a wall thickness of 13 mm. In addition, the testing conditions were different as his experiment was stopped after

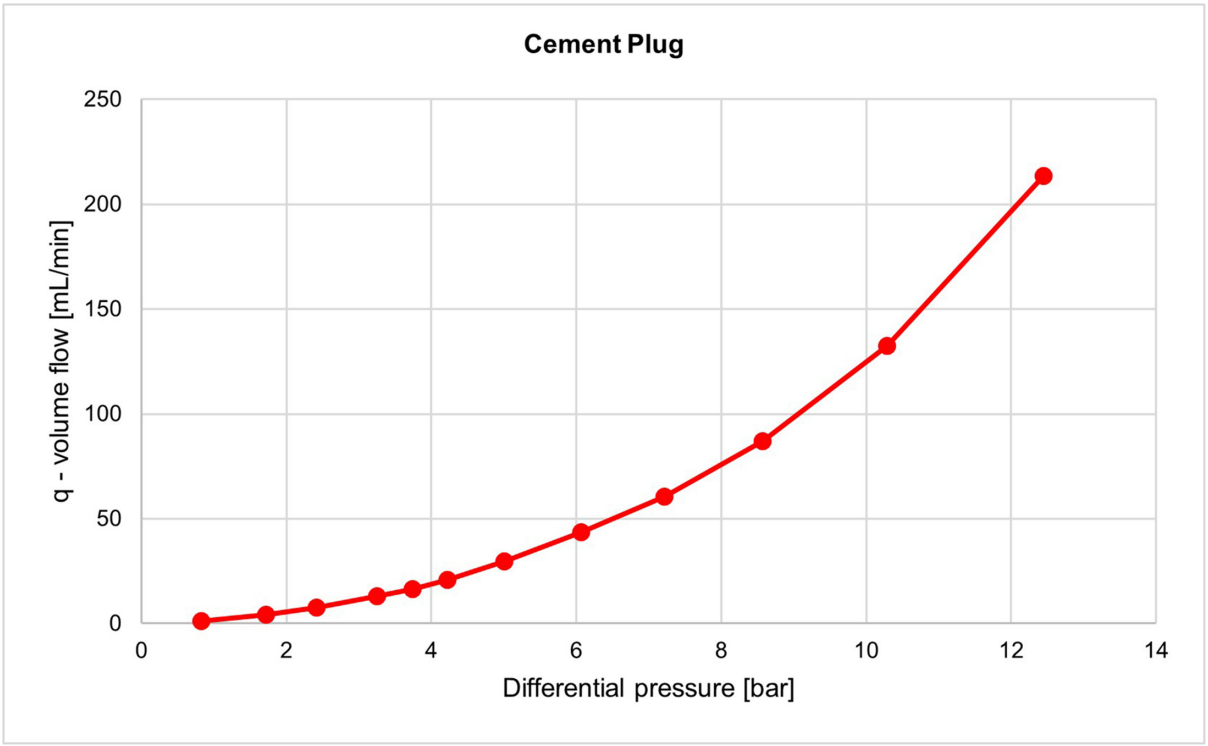

Fig. 8—Cement plug leakage test using nitrogen gas (averaged results) (Hmadeh et al. 2023b).

subjecting the plug to only 1.2 bar of differential pressure, whereas our experiment was concluded after exposing the plug to approximately 12.5 bar of differential pressure.

The 121-mm bismuth alloy samples were left to cure for 48 hours. However, Sample 1 was cured at atmospheric pressure, whereas Sample 2 was cured under 40 bar. **Fig. 9** demonstrates the volume flow rate as a function of differential pressure for both tested samples using a unified scale.

Alloy Sample 1 started leaking at a differential pressure of 2.1 bar, which is 1.3 bar higher than that recorded with the cement plug. It is also important to remember that the bismuth plug is also 64 mm shorter than the cement plug previously tested. Furthermore, Sample 1 showed lower leakage rates, with a maximum of 16.6 mL/min at 20 bar differential pressure, whereas the cement sample had a maximum of 213.6 mL/min at 20 bar differential pressure.

Looking at Sample 2, solidified and cured under 40 bar, no leakage was witnessed throughout the entire testing of the sample. This demonstrates the effect of setting the plug under pressure, in which radial expansion was induced, thus providing better sealability across the pipe-plug interface. It is worth noting that if the pipe wall is thin, then more radial expansion is induced. Therefore, even after applying a differential pressure of 20 bar, the plug sample remained intact, and the nitrogen gas could not create a leakage pathway neither across the plug-pipe interface nor through the bulk of the plug (as it is impermeable).

To enhance the comparison of the leakage rates (i.e., the slope of the curves) observed in both alloy Sample 1 and cement at once, it was optimal to merge them into a single graph using a consistent scale as projected in **Fig. 10.** It is worth noting that alloy Sample 2 was excluded from this comparison as it was cured under different conditions. From the graphs projected in **Fig. 10**, one can note that the graph of alloy Sample 1 has a substantially flatter slope, indicating lower leakage rates as a function of increasing differential pressure. Again, taking the worst-case scenario and if the slopes represent the order of magnitude between the cement plug and bismuth alloy plug (Sample 1), the alloy plug would have on average more than 18 times the hydraulic bond strength that cement exhibits under the described testing conditions.

The results projected in this study are highly influenced by several factors and thus are subjected to enhancements depending on the factors highlighted below:

Plug Length. It was proven that plug length plays a vital role when it comes to the bond strength of the plug (Hmadeh et al., 2023a). **Fig. 11** illustrates that the hydraulic bond strength increases as the plug length increases, and thus longer plugs could be deployed if larger resistance is required in certain applications.

Curing Time. The effect of curing time is an important factor to consider as the bismuth expansion continues over time. It was verifiable through a study conducted at atmospheric pressure and temperature that a bismuth alloy plug strengthens over time, as seen in **Fig. 12.** We can then extrapolate that the same strengthening effect would most likely be observable when curing under higher pressure. This trend was more notable in the very first hours after plug solidification when a steeper slope was witnessed between 17 and 24 hours of curing time, indicating a bond strength increase of 9%. However, if we compare the bond strength of the plug after 24 hours of curing with that after 115 hours, we note a further bond strength increase of only 10%. Therefore, the effect of curing time becomes less evident as time increases, an observation that agrees with **Table 1** and 5N Inc (2012). Abrahamsen (2022) also conducted mechanical push-out experiments on bismuth alloy plugs, observing that the plug cured for 3 hours was being displaced more easily compared to the plug samples that were left to cure for 17 and 72 hours. Further considerations are necessary to determine adequate curing times in field operations.

Pipe Roughness. The roughness of the casing or pipe significantly influences the efficacy of the sealability of the plug, as well as the contact angle between the bismuth-tin alloy and steel. This assertion finds validation in the literature, which indicates that pipes with rough surfaces exhibit diminished leakage rates in contrast to smoother counterparts (Corina et al. 2020). In essence, increased pipe

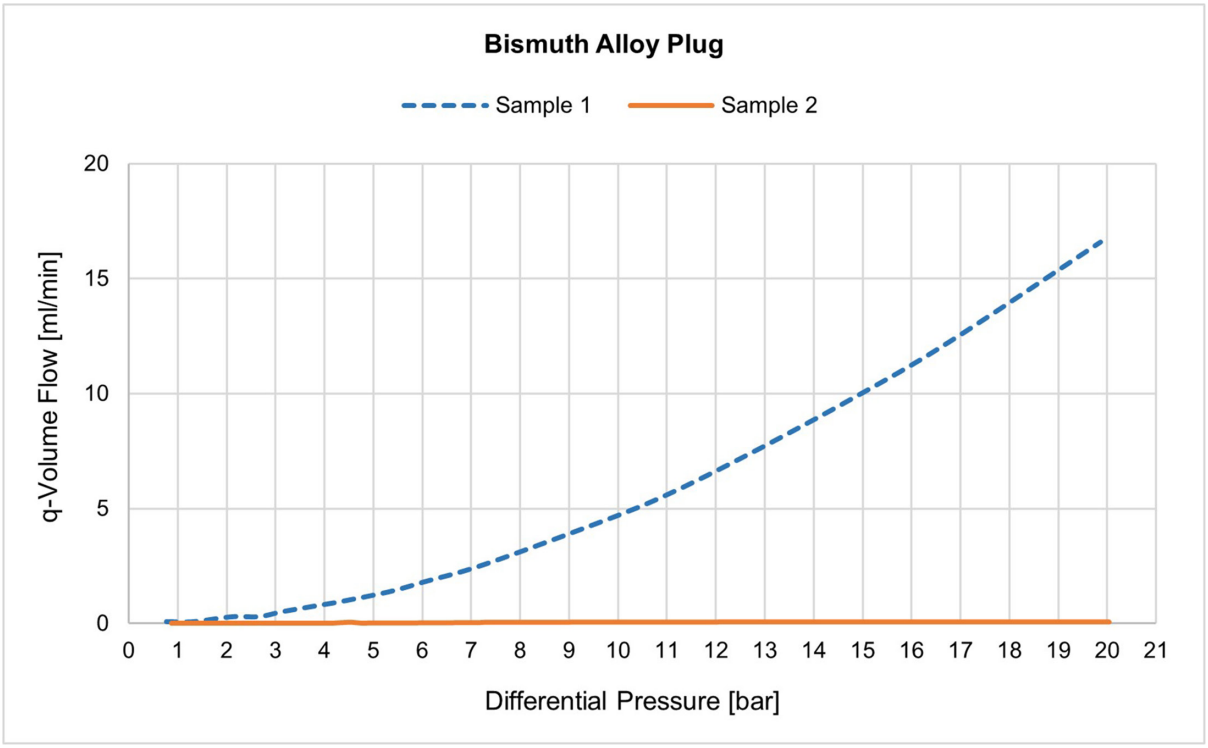

Fig. 9—Bismuth alloy plug leakage test using nitrogen gas (curing pressures: Sample 1 at 1 bar and Sample 2 at 40 bar).

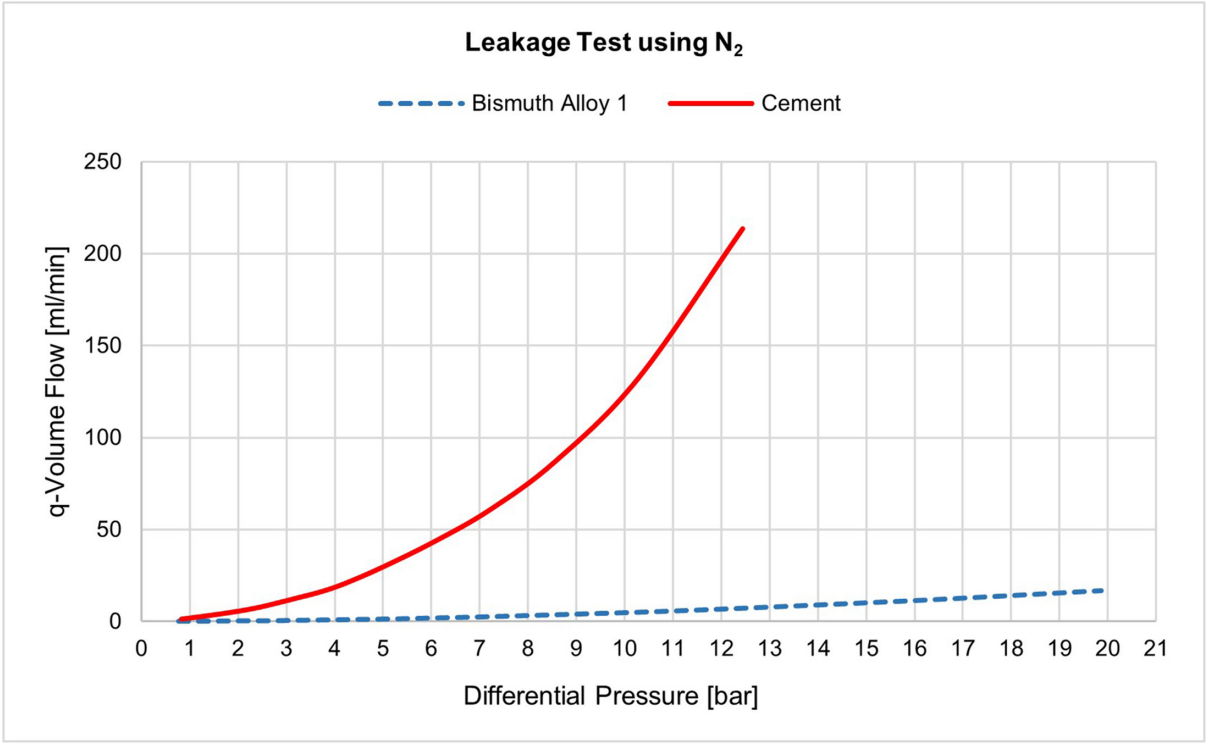

Fig. 10—Leakage test results of alloy Sample 1 and cement plug (Hmadeh et al. 2023b).

roughness directly correlates with enhanced seal performance of the metallic alloy plug. This factor is scheduled for more in-depth investigation in an upcoming series of experiments.

Microstructure Analyses. The micrographs taken using the SEM analysis are depicted next. Different locations from each sample were studied to obtain more conclusive and comparative results. The SEM images from Sample 1—cured under atmospheric pressure for 48 hours—are depicted in **Fig. 13,** whereas those of Sample 2—cured under 40 bar of pressure for 48 hours—are depicted in **Fig. 14.** The

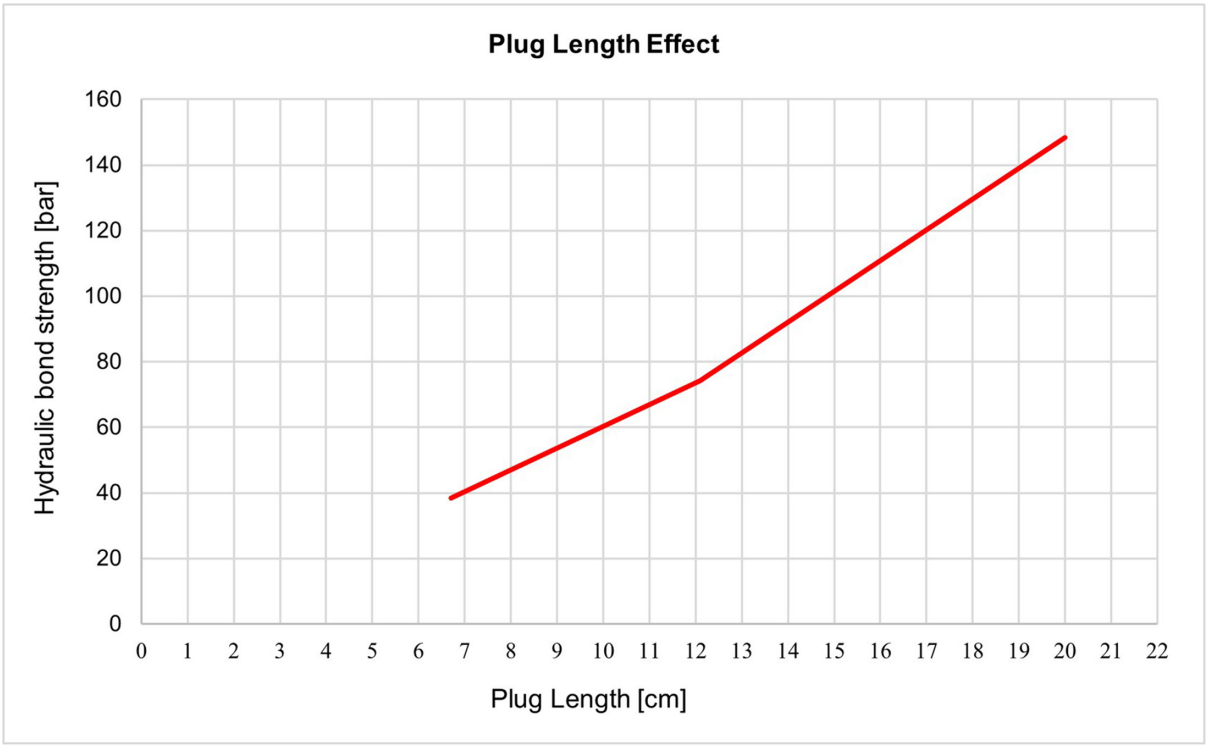

Fig. 11—The variation of hydraulic bond strength (bar) as a function of plug length (cm) (Hmadeh et al. 2023a).

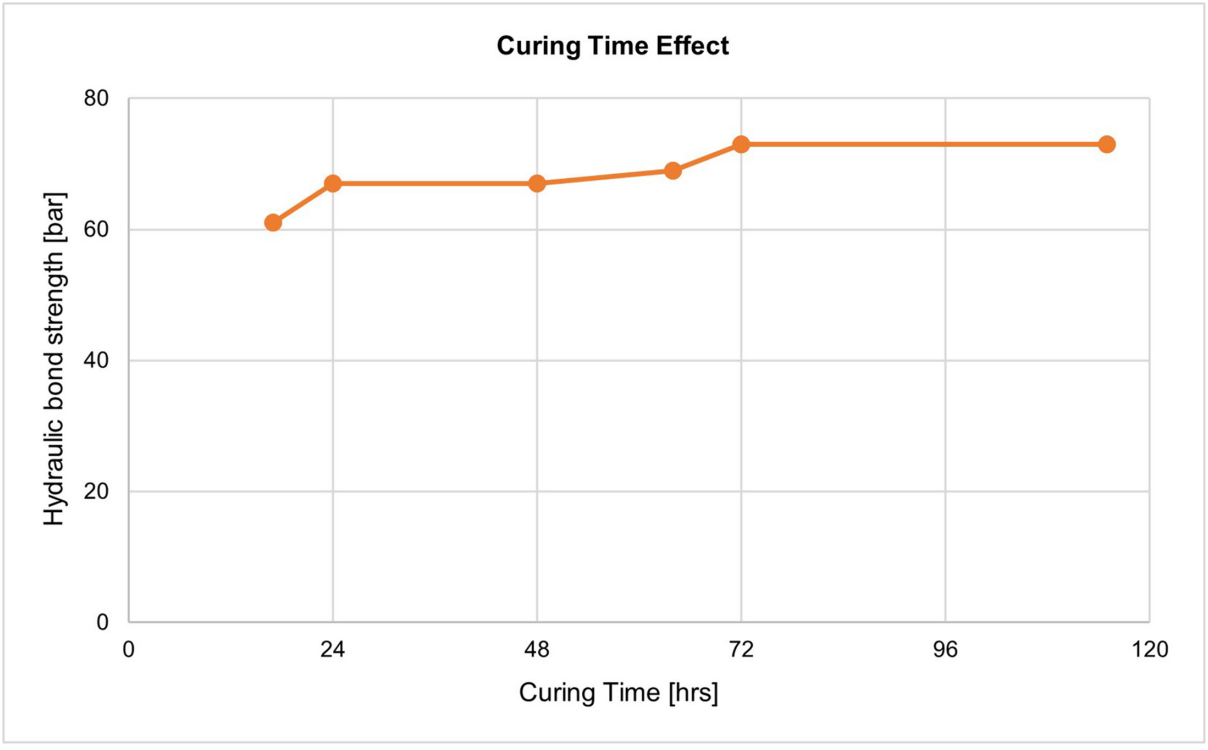

Fig. 12—Effect of curing time on the bond strength of bismuth alloy plug samples (adapted from Hmadeh et al. 2023b).

coordinates of SEM images taken from the first sample are nearly identical to those taken from the second sample. Location A in both samples are exactly on the interface between the BiSn alloy and the wall of the steel mold. Location E is in the center of the samples, while Locations B, C, and D are randomly picked as identical points within the samples.

In the SEM images, the darker contrast represents tin, which is the lighter element of the alloy, and the brighter contrast corresponds to phases rich in bismuth as it is the heavier element (Bozinovic et al. 2021; Manataki et al. 2023; Mei and Morris 1992; Silva et al. 2015). The eutectic BiSn alloy consists of two phases arranged in plates that are not flat, resulting in a complicated microstructure, known as

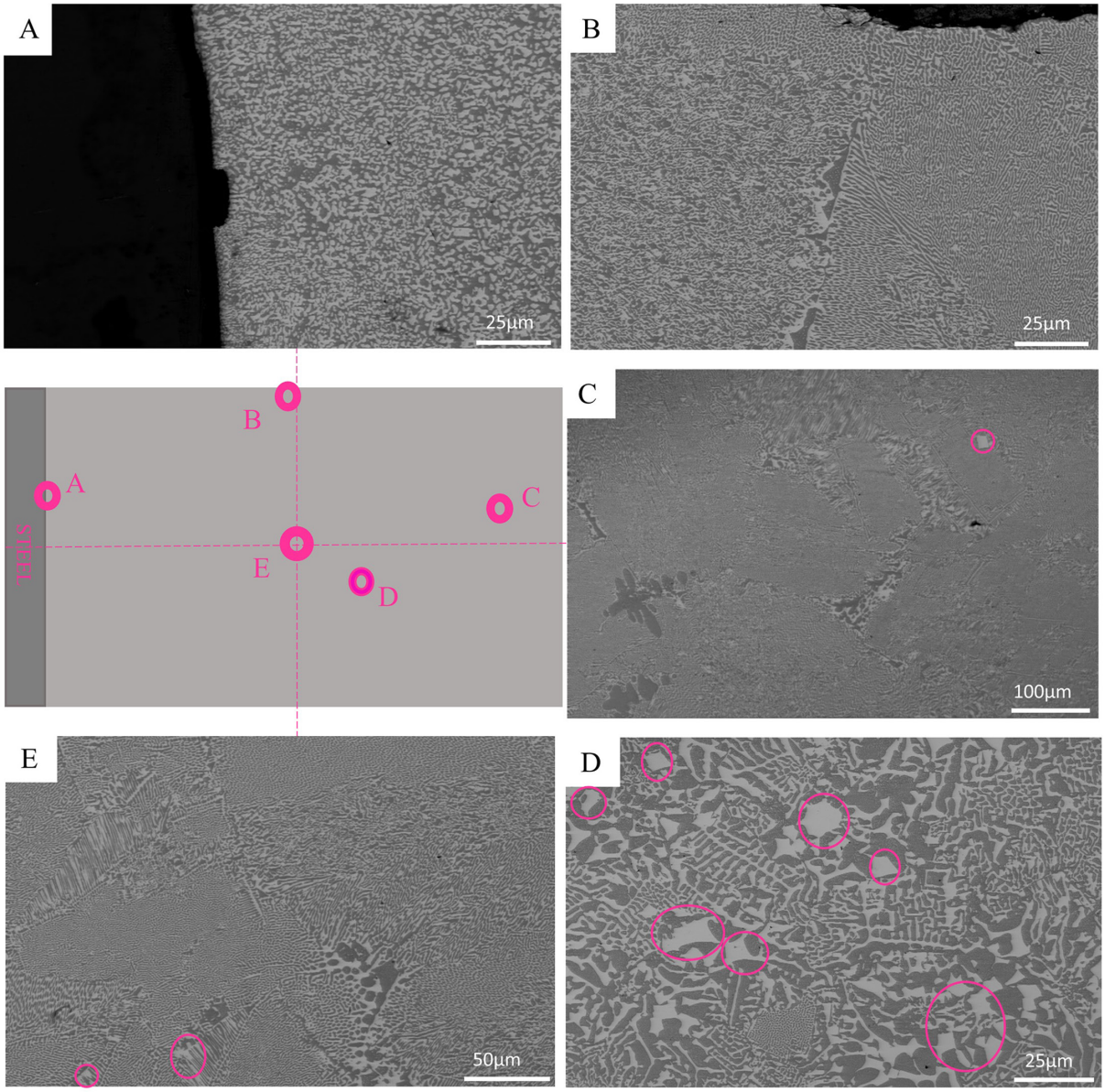

Fig. 13—SEM images from Sample 1, cured under atmospheric pressure.

"Chinese script." The microstructure is also often referred to as a complex regular structure, with one phase being a zone of regular repeating patterns, and the other phase being a zone of random irregular orientations (Bozinovic et al. 2021; Manataki et al. 2023). In some studies, the microstructure is also characterized as an irregular lamellar structure with a mixture of sharp lines, typically of rhombohedral crystals of brittle bismuth and body-centered tetragonal ductile β-tin phases (Bozinovic et al. 2021; Manataki et al. 2023; Silva et al. 2015). More details of the eutectic BiSn alloy microstructure are found in Manataki et al. (2023).

Sample 1 conveyed in **Fig. 13** has both fine and coarse patterns, with the coarser patterns seemingly dominating the sample's microstructure. Many coarsened Bi crystals (circled in pink) are specifically observed in the microstructure. Then, Sample 2 depicted in **Fig. 14** reveals that it has a finer microstructure with more densely packed arrangements and with just a few brittle Bi crystals (circled in yellow), in comparison with the microstructure of the first sample. As it is known, materials with finer microstructures exhibit better mechanical properties, particularly in terms of yield strength, compared to those with coarser grain microstructures (Callister and Rethwisch 2014). Finer grain size means more grain boundaries, which in turn enhances resistance to dislocation. Dislocation represents the capacity of the grain to move unrestrictedly within a material, causing its plastic deformation. Materials with finer grains exhibit greater hardness and higher yield strength compared to those with coarser grains. Therefore, Sample 2 should exhibit better mechanical properties than Sample 1. Another consideration is the presence of many coarsened Bi-rich phases in the first sample; this is a concern because Bi crystals are generally brittle in nature, and they can thus result in poor mechanical properties of the plug. This observation again emphasizes Sample 2 as the best candidate for obtaining better mechanical properties. The results from the characterization of the microstructure of the two samples align with the results of the hydraulic pressure tests and explain why Sample 2 withstood higher hydraulic pressure than Sample 1.

Numerical Simulations. Fig. 15 illustrates the bismuth plug inserted into the steel pipe, as modeled on Ansys. The dimensions for this geometry are the same as in the laboratory tests and are summarized in **Table 3.** Our intention is to use the laboratory tests to observe how

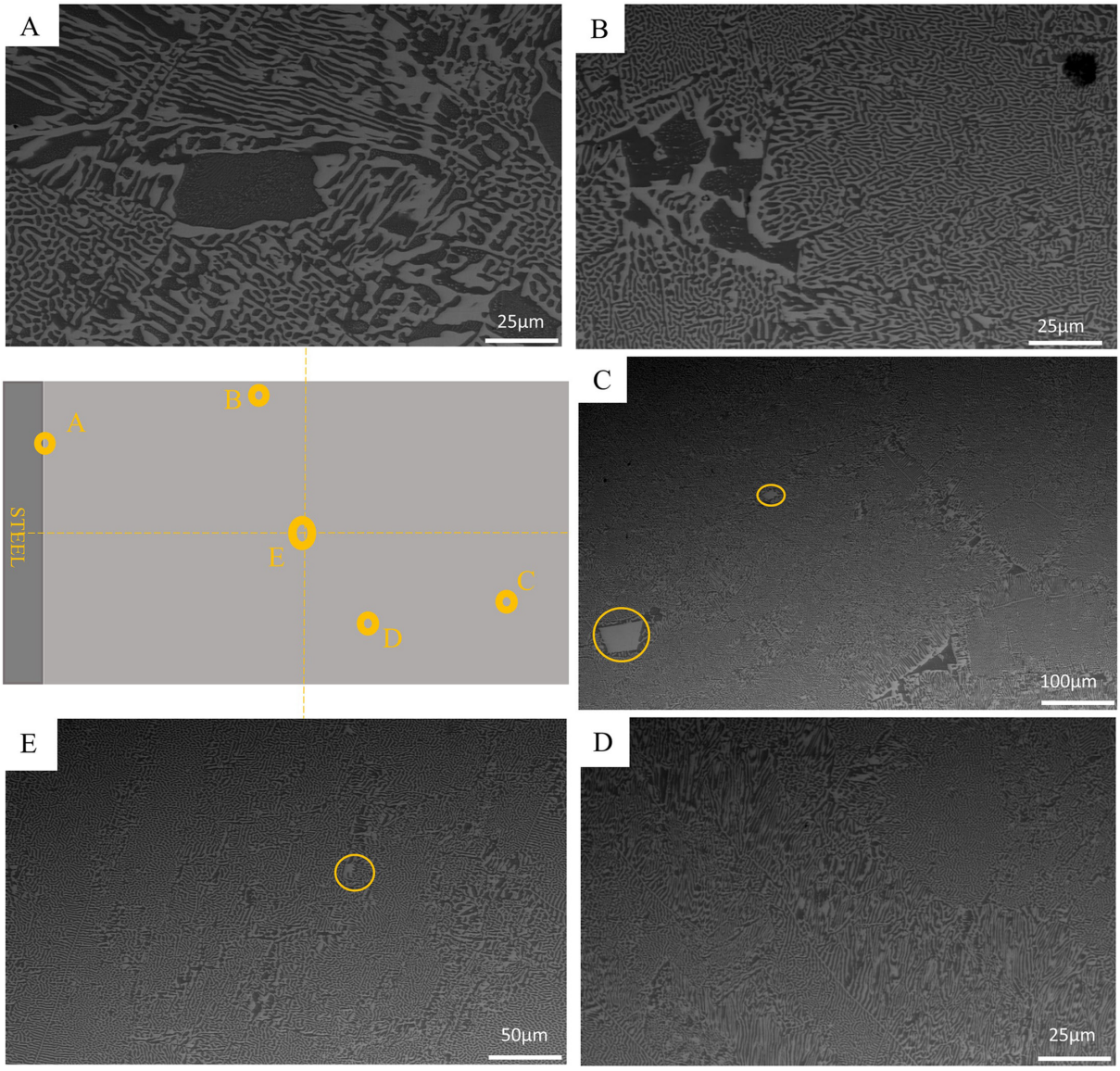

Fig. 14—SEM images from Sample 2, cured under 40 bar.

our numerical model behaves so that in the future it can be extended to other geometries and downhole conditions. Custom materials—namely Eutectic Bismuth-Tin Alloy and Steel X-52—are assigned to the plug and pipe, respectively. The software automatically detects the contact between the pipe and the plug, which we set as a frictional contact. The contact between the plug and the pipe's inner wall happens due to the plug expanding and deforming the pipe. This type of contact allows separation between the two touching surfaces and allows sliding to occur between them, according to a defined friction coefficient that is set to 0.3 initially, a common value for friction between two metals (Blau 2009). Further frictional studies are necessary to confirm the adopted friction coefficient. Finally, we know that the coefficient of thermal expansion of the bismuth alloy is higher than the one for steel, and thus one would expect that a radial gap starts to build up as we decrease the temperature of this assembly; however, the expansion and creep behavior of the alloy itself counterbalance this effect to secure the sealability.

Dimension	Value
Pipe outer diameter	60.80 mm
Pipe inner diameter	53.35 mm
Plug diameter	53.35 mm
Pipe length	250 mm
Plug length	121 mm
Distance from pipe top to plug top	34 mm
Distance from plug bottom to pipe bottom	95 mm

Table 3—Dimensions of the problem geometry.

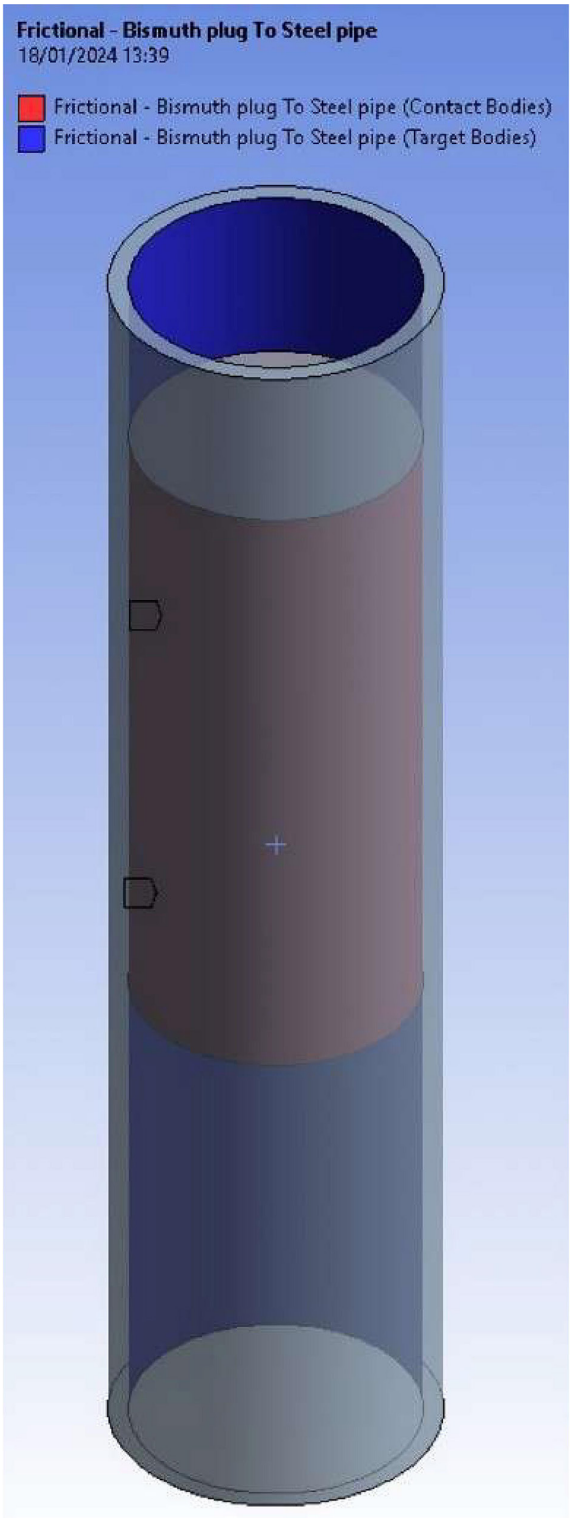

Fig. 15—Problem geometry, as seen on Ansys.

We simulate to verify the adhesion between the pipe and the plug as this assembly is cooled down. Note that this model includes the expansion upon solidification effect previously described. **Fig. 16** shows how the average gap increases as the temperature decreases by comparing the average radial deformations of the plug and the pipe. The gap curve is obtained by subtraction of the pipe and plug curves. We note that the curve for the plug has a slightly higher slope than the curve for the pipe, which is a consequence of the higher coefficient of thermal expansion of bismuth compared to steel. The average gap is negative, which means that the plug is in contact with the pipe inner wall, but is increasing, which means that contact is reducing as the temperature of the assembly decreases.

At this stage, long-term temperature effects such as creep and aging effects are not considered. By maintaining the plug under a compressive axial load for a certain period of time, which is the case when the samples are being cured under pressure, it is expected that it will experience some further radial deformation due to creep, thus reducing the radial gap. Closing the gap is fundamental for this application, as wider gaps allow for more leakage through the radial space as well as adhesion reduction between the two surfaces. Temperature

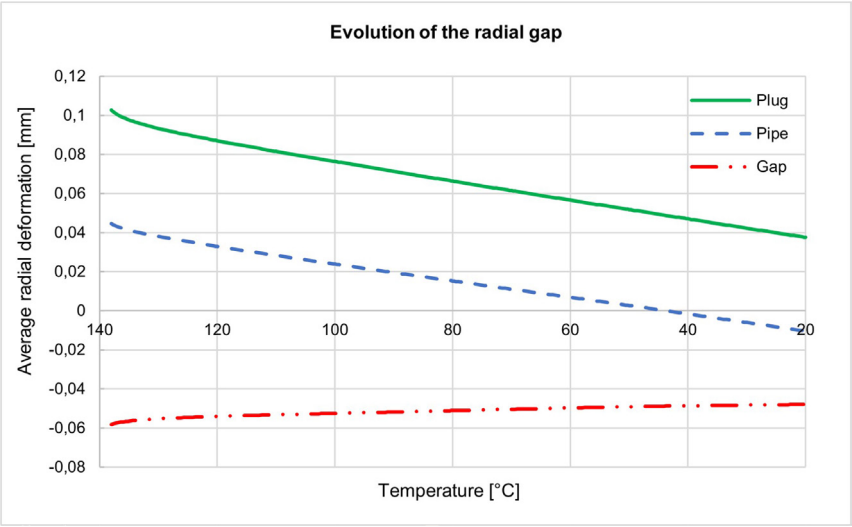

Fig. 16—Effect of the temperature on the radial gap between pipe and plug.

effects are intended to be incorporated with more detail in subsequent studies to accompany laboratory tests under varying curing temperatures.

Conclusions

The purpose of these experimental and simulation studies is to gain a better understanding of the sealing ability of eutectic bismuth-tin plugs. The main conclusions drawn from this study are the following:

- Both hydraulic push-out tests and leakage tests using nitrogen gas indicated that bismuth alloy plugs have higher resistance to applied pressure and reduced gas migration in the microannuli compared to cement, thus displaying better sealability. This outcome is applicable solely within the context of the selected plug-length scale. To accurately extend laboratory findings to actual wellbores, a thorough scalability analysis is required.
- No nitrogen leakage was witnessed while testing the bismuth alloy sample that was set under 40 bar of pressure. The exerted pressure on top of the plug created a compressive force on the plug which helped achieve a better seal by pushing the plug to expand in the radial direction.
- The microstructure characterization was also able to verify the reason behind the better performance of a bismuth plug set under pressure compared to that set under atmospheric pressure, in which findings revealed more brittle bismuth structures in the latter.
- The sealing effectiveness of a bismuth alloy plug can be influenced by various factors, including curing duration, plug length, the surface roughness of the pipe being set in, and the placement efficiency. Increased curing time, longer plug length, a rougher pipe surface, and a proper placement contribute favorably to the plug sealing performance.
- Numerical simulations carried out managed to capture the expansion upon solidification effect of bismuth, as well as understanding the adhesion between the bismuth alloy and steel. Further modeling is necessary to capture long-term temperature effects (creep, aging), which will then be coupled with further laboratory tests.

Despite the knowledge collected regarding bismuth alloy plugs, it remains quite early to discuss the qualification of this technology. Qualifying these metal plugs poses challenges, particularly given the prevailing reliance on cement, which remains a familiar and comfortable choice for many operators. Nevertheless, the investigation of alternative materials could offer improved sealing quality, cost-effectiveness by reducing rig time for well plugging, and environmental benefits through corrosion resistance, nontoxicity, and a low carbon footprint. It is still early to affirm if bismuth plugs will manage to address all these aspects, as more field tests are necessary for further qualification. New materials, once qualified, are not intended to replace cement for good but instead to support it as alternatives in specific scenarios. Alternatively, a combined sealing approach using both materials—a shortened cement plug with a bismuth alloy plug on top—could offer better sealing assurance and a cost-effective solution. Given that each plug has distinct failure mechanisms, this strategy might pave the way for more reliable and enduring well plugging solutions.

Finally, achieving the qualification of bismuth alloy plugs requires further scrutiny through monitored field applications, as exemplified by ongoing efforts by AkerBP in setting and monitoring the performance of bismuth alloy plugs. This approach provides valuable insights into the real-world performance of the plug under diverse well conditions.

Acknowledgment

The authors acknowledge the Research Council of Norway (RCN) for financing the Center for Research-based Innovations "SWIPA - Center for Subsurface Well Integrity, Plugging and Abandonment," RCN project no. 309646, for which the work has been carried out. The center is also financed by the operating companies AkerBP, Equinor ASA, and Wintershall Dea Norway, and includes, in addition, more than 20 in-kind contributing industry partners. The R&D partners in SWIPA are SINTEF, NORCE, IFE, NTNU and UiS. The authors would like to thank the team at SINTEF (Drilling & Wells) who helped in preparing cement samples and conducting leakage tests using nitrogen gas. A special thanks goes to Noralf Vedvik for all his efforts put into this work and to Andreas Elmer Abrahamsen for contributing with early experiments.

References

5N Inc. 2012. Product Data Sheet MCP 137/Metspec 281 Alloy. www.5nplus.com.

Abrahamsen, A. E. 2022. *Experimental Testing of Bismuth Alloys for Well Plugging and Abandonment*. MSc thesis, Norwegian University of Science and Technology.

API, RP 10B-2, *Recommended Practice for Testing Well Cements*. 2013. Washington D.C., USA: API.

Blau, P. J. 2009. *Friction Science and Technology, From Concepts to Applications*. Milton Park, USA: Taylor & Francis.

Bozinovic, K., Manasijevic, D., Balanovic, L. et al. 2021. Study of Microstructure, Hardness and Thermal Properties of Sn-Bi Alloys. *Hem Ind* **75** (4): 227–239. doi:https://doi.org/10.2298/HEMIND210119021B.

Callister, W. D. and Rethwisch, D. G. 2014. *Materials Science and Engineering An Introduction*, 9th ed. Hoboken, New Jersey, USA: Wiley.

Carragher, P. and Fulks, J. 2018. A New Look at Sealing with Bismuth and Thermite. Paper presented at the SPE Annual Technical Conference and Exhibition, Dallas, Texas, USA, 24–26 September. https://doi.org/10.2118/191469-MS.

Carragher, P., Fulks, J., and McWilliam, G. 2019. Rigless Solutions to Well Intervention with Bismuth and Thermite. Paper presented at the SPE/IADC International Drilling Conference and Exhibition, The Hague, The Netherlands, 5–7 March. https://doi.org/10.2118/194174-MS.

Corina, A. N., Opedal, N., Vrålstad, T. et al. 2020. The Effect of Casing-Pipe Roughness on Cement-Plug Integrity. *SPE Drill & Compl* **35** (2): 237–251. doi:https://doi.org/10.2118/194158-PA.

Dusseault, M. B., Gray, M. N., and Nawrocki, P. A. 2000. Why Oilwells Leak: Cement Behavior and Long-Term Consequences. Paper presented at the International Oil and Gas Conference and Exhibition in China, Beijing, China, 7–10 November. https://doi.org/10.2118/64733-MS.

Eden, R. D. 2005. Sealing Method and Apparatus. Patent US20050199307A1. https://patentimages.storage.googleapis.com/0c/92/eb/ffd83e30c31637/US20050199307A1.pdf.

Fulks, J. and Carragher, P. 2021. Squeezing Perforations Rigless – No Pumping or Injection Required. Paper presented at the SPE/ICoTA Well Intervention Conference and Exhibition, Virtual, 22–25 March. https://doi.org/10.2118/204404-MS.

Goodrich, W. E. 1929. Volume Changes during the Solidification of Metals and Alloys of Low Melting-Point. *Trans Faraday Soc* **25**: 531–569. doi:https://doi.org/10.1039/tf9292500531.

Hetlevik, S. 2022. *International Market Development and Operations, Challenges and Possibilities*. Sandnes, Norway: Flo Petrol Well Barrier AS.

Hmadeh, L., Anunciação Jaculli, M., Elahifar, B. et al. 2024. Development of Bismuth-Based Solutions for Well Plugging and Abandonment: A Review. *Pet Res*. doi:https://doi.org/10.1016/j.ptlrs.2024.01.003.

Hmadeh, L., Elahifar, B., and Sangesland, S. 2023a. The Sealing Behavior of Bismuth-Based Metal Plugs. Paper presented at the ASME 2023 42nd International Conference on Ocean, Offshore and Arctic Engineering, Melbourne, Australia, 11–16 June. https://doi.org/10.1115/OMAE2023-104309.

Hmadeh, L., Elahifar, B., Sangesland, S. et al. 2023b. A Full Laboratory Study on the Physical and Mechanical Properties of A Bismuth Plug. Paper presented at the SPE/IADC International Drilling Conference and Exhibition, Stavanger, Norway, 7–9 March. https://doi.org/10.2118/212561-MS.

Khairulin, R. A., Stankus, S. V., Abdullaev, R. N. et al. 2010. The Density and Interdiffusion Coefficients of Bismuth-Tin Melts of Eutectic and near-Eutectic Composition. *High Temp* **48** (2): 188–191. doi:https://doi.org/10.1134/S0018151X10020082.

Kilic, S., Kacar, I., Sahin, M. et al. 2019. Effects of Aging Temperature, Time, and Pre-Strain on Mechanical Properties of AA7075. *Mat Res* **22** (5). doi:https://doi.org/10.1590/1980-5373-mr-2019-0006.

Mackenzie, G., McLelland, A., Carragher, P. et al. 2022. Innovative and Collaborative Well Intervention Solution Restores Well Integrity to Compromised Completion. Paper presented at the SPE/ICoTA Well Intervention Conference and Exhibition, The Woodlands, Texas, USA, 22–23 March. https://doi.org/10.2118/209036-MS.

Manataki, A., Kontis, P., and Sangesland, S. 2023. Investigation of the Microstructure of Bismuth Alloy and Its Interaction With Cement and Steel Casing. Paper presented at the ASME 2023 42nd International Conference on Ocean, Offshore and Arctic Engineering, Melbourne, Australia, 11–16 June. https://doi.org/10.1115/OMAE2023-103843.

Mei, Z. and Morris, J. W. 1992. Characterization of Eutectic Sn-Bi Solder Joints. *J Electron Mater* **21** (6): 599–607. doi:https://doi.org/10.1007/BF02655427.

NORSOK D-010, *Well Integrity in Drilling and Well Operations Rev*. 2021, Vol. 5. Lysaker: Standard Norge.

Offshore Norge. 2021. *Roadmap for New P&A Technology*. Offshore Norge. https://www.offshorenorge.no/contentassets/a068553616694ca18fbb0acd5646d4e6/pa-roadmap-paf----final-100221.ppt.pdf.

Opedal, N., Corina, A. N., and Vrålstad, T. 2018. Laboratory Test on Cement Plug Integrity. Paper presented at the ASME 2018 37th International Conference on Ocean, Offshore and Arctic Engineering, Madrid, Spain, 17–22 June. https://doi.org/10.1115/OMAE2018-78347.

Roijmans, R. F. H., Wolterbeek, T. K. T., Cornelissen, E. K. et al. 2023. Evaluating the Sealing Performance of Plug and Abandonment Cement Systems Under Downhole Conditions. *SPE J.* **28** (6): 2737–2752. doi:https://doi.org/10.2118/212542-PA.

Rolf Lycke AS. 2012. *Seamless Steel Pipe for Offshore Applications in API 5L X52 Modified*. (accessed 20 October 2023).

Silva, B. L., Reinhart, G., Nguyen-Thi, H. et al. 2015. Microstructural Development and Mechanical Properties of a Near-Eutectic Directionally Solidified Sn–Bi Solder Alloy. *Mater Charact* **107**: 43–53. doi:https://doi.org/10.1016/j.matchar.2015.06.026.

Thorstensen, E., Vadset, K., Straume, M. K. et al. 2022. Bismuth Plugs Used to Cap All Wells During the Final Phase of the Valhall DP Abandonment Campaign, Offshore Norway. Paper presented at the Offshore Technology Conference, Houston, Texas, USA, 2–5 May. https://doi.org/10.4043/31897-MS.

Vrålstad, T., Saasen, A., Fjær, E. et al. 2019. Plug & Abandonment of Offshore Wells: Ensuring Long-Term Well Integrity and Cost-Efficiency. *J Pet Sci Eng* **173**: 478–491. doi:https://doi.org/10.1016/j.petrol.2018.10.049.

Vrålstad, T., Skorpa, R., Opedal, N. et al. 2015. Effect of Thermal Cycling on Cement Sheath Integrity: Realistic Experimental Tests and Simulation of Resulting Leakages. Paper presented at the SPE Thermal Well Integrity and Design Symposium, Banff, Alberta, Canada, 23–25 November. https://doi.org/10.2118/178467-MS.

Vrålstad, T., Todorovic, J., Saasen, A. et al. 2016. Long-Term Integrity of Well Cements at Downhole Conditions. Paper presented at the SPE Bergen One Day Seminar, Grieghallen, Bergen, Norway, 20 April. https://doi.org/10.2118/180058-MS.

Zhang, H., Ramakrishnan, T. S., Elias, Q. K. et al. 2020. Evaluation of Bismuth-Tin Alloy for Well Plug and Abandonment. *SPE Prod & Oper* **35** (1): 111–124. doi:https://doi.org/10.2118/199363-PA.

Zhang, H., Ramakrishnan, T. S., Elkady, Y. M. et al. 2021a. Comparative Evaluation of Bismuth-Silver and Bismuth-Tin Alloys for Plug and Abandonment. *SPE Drill & Compl* **36** (2): 368–382. doi:https://doi.org/10.2118/202488-PA.

Zhang, C., Wang, C., Zhang, S. L. et al. 2021b. Effect of Aging Temperature on the Precipitation Behavior and Mechanical Properties of Fe–Cr–Ni Maraging Stainless Steel. *Materials Sci Eng: A* **806**: 140763. doi:https://doi.org/10.1016/j.msea.2021.140763.